Spin-orbital effect on the polariton state in traps

Yuri G. Rubo [*]

Instituto de Energías Renovables, Universidad Nacional Autónoma de México, Temixco, Morelos 62580, Mexico

I discuss the similitude and differences in spin-orbital effects for electrons in quantum wells with Rashba coupling and for polaritons in semiconductor microcavities with transverse-electric–transverse-magnetic (TE-TM) splitting. In contrast to the case of electrons, the ground state of polaritons in the trap can be nondegenerate and can possess a specific polarization structure. For the case of an azimuthally symmetric trap and sufficiently strong spin-orbital coupling, the ground state is either a radial or an azimuthal vortex, depending on the sign of the coupling constant. The effect is strongly enhanced for polaritons trapped in a ring, where even weak TE-TM splitting results in the formation of vorticity and definite polarization of the ground state. The Hamiltonian for quasi-one-dimensional motion of polaritons in the ring is derived, and it is shown that the dispersion of polaritons depends qualitatively on the curvature of the ring.

I. INTRODUCTION

Rashba spin-orbital coupling (SOC) [1,2] and the discovery of electric-dipole spin resonances [3,4] played a pivotal role in our understanding of spin-dependent phenomena in bulk semiconductors. The role of SOC is even more pronounced in low-dimensional semiconductor structures, where the Rashba [5,6] and the Dresselhaus [7] terms, which are both linear in the wave vector in quantum wells, allow effective manipulation of electron spins by an electric field [8]. These discoveries have founded in part the study of spintronics [9,10], have a huge influence on the development of quantum computing with semiconductor quantum dots, and have a pronounced impact on other areas of condensed matter physics [11].

This influence resulted, in an especially evident and straightforward manner, in the development of research and applications of exciton-polariton condensates in semiconductor microcavities. The strong coupling of light with excitons in semiconductors was first discussed in pioneering work by Pekar in 1957 [12], which led him to the discovery of additional light waves, and quanta of these waves are referred to as polaritons nowadays. Polaritons, due to their excitonic component, are interacting quasiparticles, both with phonons and with themselves, and they are sensitive to external fields, which in principle allows their manipulation in the crystal. While efficient relaxation of polaritons in bulk crystals can take place, Bose-Einstein condensation in its original sense is not possible: The lower polariton branch is photonlike at low energies, and it does not have a ground state to condense to [13]. (The same argument is known for blackbody radiation [14,15].) The situation is different in two-dimensional (2D) semiconductor microcavities [16], where polariton condensates have been discovered [17–19] and intensively investigated in recent years.

Semiconductor microcavities are made of a semiconductor layer, that is a few micrometers thick, placed between two distributed Bragg mirrors to hold a specific mode of light trapped in the growth direction. Several semiconductor quantum wells are also put in the antinodes of the light mode, in order to provide strong coupling of the light with excitons in quantum wells, resulting in the formation of lower and upper polariton branches. As long as only the lower polariton branch is of interest, the polariton states in a microcavity are similar to the 2D electron states, in the sense that both are described by two-component wave functions. On the one hand, many polarization effects and phenomena observed and discussed for the polariton system are to some extent copycats of those for electrons in quantum wells, but on the other hand, they frequently bring in new ideas related to higher space and time coherence of polaritons and to the feasibility of experimental observation and verification by optical means. It is worth mentioning the optical spin Hall effect [20,21], the polariton Berry-phase interferometer [22], and the polariton *Zitterbewegung* [23,24] as some examples of effects that rely heavily on the presence of strong coupling between orbital and pseudospin dynamics in polariton transport (see also the review in Ref. [25] and references therein for additional information). The linear-in-the-wave-vector SOC can be regarded as a vector potential with noncommuting components, or the non-Abelian gauge field, and the related effects can be clearly demonstrated by optical means [26].

More recently, there has been growing interest in applications of polariton condensates for analog and quantum computation. The task of forming a well-defined two-level system with polaritons is noticeably more complex than it is for electrons in semiconductor low-dimensional quantum systems. Even in the single-particle approximation the energy levels of a trapped polariton are qualitatively different from those of an electron. The main difference comes from the role

_____
[*]ygr@ier.unam.mx

played by the time-reversal symmetry (TRS). For electrons the time-reversal operator $\mathcal{T}_e$ is odd, $\mathcal{T}_e^2 = -1$, which ensures at least double degeneracy of all electron levels in the case when TRS is present. This fact, known as the Kramers theorem [27], allows one, in principle, to address a particular Kramers doublet for qubit operations. In contrast, the polaritons are composite bosons and the time-reversal operator for them, $\mathcal{T}_p$, is even, $\mathcal{T}_p^2 = 1$, which does not guarantee the degeneracy of energy levels.

The condition of TRS imposes limitations on possible spin-orbit synthetic Hamiltonians [28] which can be obtained for polaritons and limits substantially the analogy between electron and polariton systems. This is a clear reflection of the fact that polaritons are described by pseudospin, rather than the real spin. In particular, the Rashba term cannot appear in the polariton Hamiltonian with preserved TRS. Interestingly, however, the so-called Rashba-Dresselhaus term, which corresponds to the case when the Rashba and the Dresselhaus contributions have the same amplitude [29], is allowed for both electrons and polaritons, which provides identical Hamiltonians with SU(2) symmetry and allows the formation of a persistent spin helix [29,30]. Having this in mind, the term "spin-orbital coupling" is used for the polariton system in what follows.

In this paper, the energy levels of polaritons in azimuthally symmetric traps are considered. It is shown that the ground state can become a singlet in the case where the SOC is strong enough. The ground-state singlet is characterized by well-defined radial or azimuthal linear polarization. This effect turns out to be especially strong for polaritons trapped in the rings, and since this configuration has received much interest recently [31–35], the SOC for the motion of polaritons in the ring is studied in more detail. To highlight the effects of SOC, the consideration is carried out neglecting dissipation, i.e., assuming infinite lifetimes of polaritons in the traps. This approximation is acceptable for ultrahigh-quality microcavities [35,36], with the polariton lifetimes exceeding 100 ps.

The equations for the case of SOC due to transverse-electric–transverse-magnetic (TE-TM) splitting in axially symmetric traps are formulated in Sec. II below. The energy levels of parabolic and hard-wall disk traps are considered in Sec. III. Section IV is devoted to the important case of ring traps. The conclusions are given in Sec. V.

II. BASIC EQUATIONS

A polariton mode in a microcavity is fully described by the in-plane component of the electric field **E**, and it is convenient to use the 2D complex vector $\boldsymbol{\psi} = \{\psi_x, \psi_y\} \propto \mathbf{E}$ normalizing

it to the number of polaritons belonging to the mode. In the cylindrically symmetric case, the kinetic energy density near the bottom of the lower polariton branch should contain two invariants, $|\boldsymbol{\nabla} \cdot \boldsymbol{\psi}|^2$ and $|\boldsymbol{\nabla} \times \boldsymbol{\psi}|^2$. As a result, the Schrödinger equation is written as

$$
-\frac{\hbar^2}{2m_t}(\boldsymbol{\nabla} \cdot \boldsymbol{\nabla})\boldsymbol{\psi} - \frac{\hbar^2}{2}\left(\frac{1}{m_l} - \frac{1}{m_t}\right)\boldsymbol{\nabla}(\boldsymbol{\nabla} \cdot \boldsymbol{\psi})
$$
$$
= [E - U(\mathbf{r})]\boldsymbol{\psi}. \tag{1}
$$

Here, $U(\mathbf{r})$, with $\mathbf{r} = \{x, y\}$ being the 2D position, is the potential energy, and m_l and m_t are the longitudinal and the transverse effective masses of polaritons, respectively. For free polaritons, the transverse mass m_t corresponds to the transverse-electric (TE) mode with $(\boldsymbol{\nabla} \cdot \boldsymbol{\psi}) = 0$, while the longitudinal mass m_l corresponds to the transverse-magnetic (TM) mode with $[\boldsymbol{\nabla} \times \boldsymbol{\psi}] = 0$.

Instead of vector $\boldsymbol{\psi}$ they usually use two circular polarization components of the field $\psi_{\pm 1}$ defined by

$$
\boldsymbol{\psi} = \frac{\hat{\mathbf{x}} + i\hat{\mathbf{y}}}{\sqrt{2}}\psi_{+1} + \frac{\hat{\mathbf{x}} - i\hat{\mathbf{y}}}{\sqrt{2}}\psi_{-1} \tag{2}
$$

and combine them into the column $\Psi = (\psi_{+1}, \psi_{-1})^{\mathsf{T}}$. The 2×2 Hamiltonian corresponding to Eq. (1) is then

$$
H = \frac{\hbar^2}{2m^*}\begin{pmatrix} k_- k_+ & \gamma k_-^2 \\ \gamma k_+^2 & k_+ k_- \end{pmatrix} + U(\mathbf{r})\mathbb{1}, \tag{3}
$$

where $\mathbf{k} = -i\boldsymbol{\nabla}$, $k_{\pm} = k_x \pm i k_y$, and

$$
\frac{1}{m^*} = \frac{m_t + m_l}{2m_t m_l}, \quad \gamma = \frac{m_t - m_l}{m_t + m_l}. \tag{4}
$$

One can see that the difference in the transverse and longitudinal masses sets the SOC of polariton modes. This is the basic SOC in the system, and it is essentially the same as for pure light (see Ref. [37] for a review). The splitting parameter $\Delta_{\mathrm{LT}} = \hbar\gamma/m^*$ is also used to define the strength of SOC instead of the dimensionless coupling constant γ.

In the case of azimuthally symmetric potential energy $U(r)$, which is mainly considered below, the wave functions can be written in the general form

$$
\Psi = \begin{pmatrix} e^{i(m-1)\phi} f(r) \\ e^{i(m+1)\phi} g(r) \end{pmatrix}, \tag{5}
$$

where the integer $m = 0, \pm 1, \pm 2, \dots$ is the winding number and ϕ is the azimuth angle. Using the relations

$$
k_{\pm} e^{im\phi} f(r) = -i e^{i(m\pm 1)\phi}\left(\frac{d}{dr} \mp \frac{m}{r}\right)f(r), \tag{6}
$$

one obtains

$$
-\frac{\hbar^2}{2m^*}\left(\frac{d}{dr} + \frac{m}{r}\right)\left(\frac{d}{dr} - \frac{m-1}{r}\right)f(r) - \frac{\gamma\hbar^2}{2m^*}\left(\frac{d}{dr} + \frac{m}{r}\right)\left(\frac{d}{dr} + \frac{m+1}{r}\right)g(r) + U(r)f(r) = Ef(r), \tag{7a}
$$

$$
-\frac{\gamma\hbar^2}{2m^*}\left(\frac{d}{dr} - \frac{m}{r}\right)\left(\frac{d}{dr} - \frac{m-1}{r}\right)f(r) - \frac{\hbar^2}{2m^*}\left(\frac{d}{dr} - \frac{m}{r}\right)\left(\frac{d}{dr} + \frac{m+1}{r}\right)g(r) + U(r)g(r) = Eg(r) \tag{7b}
$$

for the radial functions $f(r)$ and $g(r)$.

Independently of the particular form of $U(r)$, some conclusions about the degeneracy of the energy levels can be drawn on the basis of time-reversal symmetry. Note that the time reversal for the linear polarization components is reduced to complex conjugation, as it should be for two independent oscillators, $\mathcal{T}_p\{\psi_x, \psi_y\} = \{\psi_x^*, \psi_y^*\}$. Therefore, in the circular polariton basis, one has $\mathcal{T}_p(\psi_{+1}, \psi_{-1})^\mathsf{T} = (\psi_{-1}^*, \psi_{+1}^*)^\mathsf{T}$ or $\mathcal{T}_p = K\sigma_x$, using the Pauli matrices $\sigma_{x,y,z}$ and the complex-conjugation operation K. This is in striking contrast to the electron case, where $\mathcal{T}_e = K\sigma_y$.

Applying $\mathcal{T}_p$ to the wave functions (5) and taking into account that the solutions of (7a) and (7b) can be chosen to be real functions, one has

$$m \to -m, \quad f \to g, \quad g \to f. \tag{8}$$

These substitutions leave the system composed of (7a) and (7b) unchanged, and this implies that the energies of the states m and $-m$ for $m \neq 0$ coincide. The $m = 0$ states, however, are the eigenstates of $\mathcal{T}_p$, and the corresponding energy levels remain nondegenerate.

The singlet solutions for $m = 0$ possess well-defined polarization patterns of the polariton field. In this case we have $g(r) = \pm f(r)$, so that polarization is linear, and the radial function satisfies the equation for a single-component system with angular momentum equal to 1,

$$-\frac{\hbar^2}{2m_{t,l}} \frac{d}{dr}\left(\frac{d}{dr} + \frac{1}{r}\right) f(r) + U(r)f(r) = Ef(r). \tag{9}$$

Here, the solutions with $g = -f$ are characterized by the transverse mass $m_t = m^*/(1 - \gamma)$ and by the azimuthal polarization field shown in Fig. 1(a), while the solutions with $g = f$ possess the longitudinal mass $m_l = m^*/(1 + \gamma)$ and the radial polarization field shown in Fig. 1(b).

The presence of these pure longitudinal and pure transverse states in the traps plays an important role in propagation of polariton wave packets and leads to the possibility of polarization rectification [38]. Note also that in the general case of arbitrary potential of the dot $U(\mathbf{r})$, e.g., for random polariton billiards, the singlet polariton states are described by a real valued vector field $\psi(\mathbf{r})$ and they are thus linearly polarized everywhere in the trap.

III. POLARITON LEVELS IN TRAPS

A quantum trap for polaritons can be approximated with a parabolic potential near its bottom, and it is natural to begin with a description of the energy levels for the case of harmonic potential $U(r) = m^*\omega_0^2 r^2/2$. The dependence of energies on the TE-TM splitting parameter γ, which measures the extent of the longitudinal and transverse mass difference (4), is shown in Fig. 1(c). The presence of SOC lifts the degeneracies of 2D harmonic oscillator levels, and the mean distance between the levels decreases with increasing γ. The overall behavior of energy levels resembles the case of parabolic quantum dots with Rashba SOC [39]. In our case the decrease in mean level spacing is because the increase in $|\gamma|$ with fixed m^* corresponds to the increase in the longitudinal effective mass m_l for $\gamma < 0$ or to the increase in the transverse mass m_t for $\gamma > 0$. In what follows we consider the latter case only.
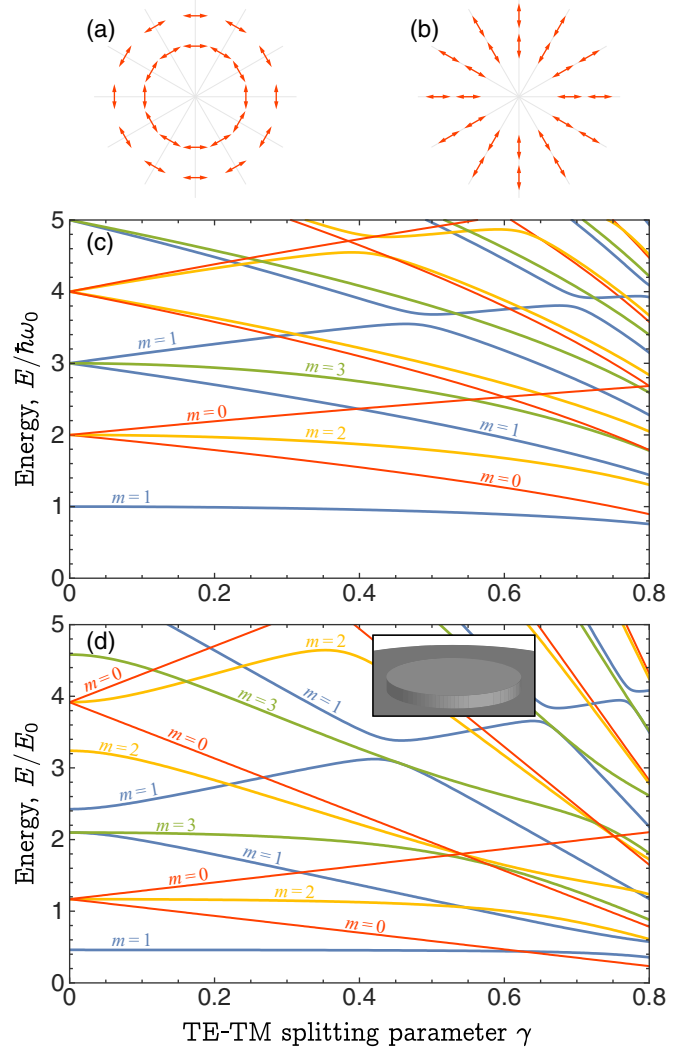

FIG. 1. The linear polarization of the states with $m = 0$, where the winding number m is defined by Eq. (5). The polarization is either azimuthal (a) or radial (b). (c) Energy levels for a 2D harmonic trap with frequency ω_0. (d) Energy levels for a hard-wall disk with radius R_0, given in units of $E_0 = \hbar^2/2\pi R_0^2 m^*$. The schematic geometry of the microcavity is shown in the inset. Blue, yellow, and green lines show the double-degenerate levels with $|m| > 0$, and red lines show the energies of the linearly polarized nondegenerate states [(a) and (b)] with $m = 0$.

Note that on the one hand the change $\gamma \to -\gamma$ corresponds to the exchange of m_l and m_t. On the other hand, $\gamma \to -\gamma$ can be compensated by the change $g \to -g$ in the system composed of (7a) and (7b). This implies 90° rotation of the polarization plane, so that the azimuthal vortices in Fig. 1(a) transform to the radial ones in Fig. 1(b) and vice versa.

While the energies of the twofold degenerate states with $|m| > 0$ are defined by some effective masses residing in between m_l and m_t, the energies of nondegenerate radial vortices are set by the lightest mass m_l, and the energies of the azimuthal vortices are defined by the heaviest mass m_t. The energies of the former states grow rapidly with increasing TE-TM parameter γ, while the energies of the latter states decrease and approach the energy of the $m = 1$ state, which
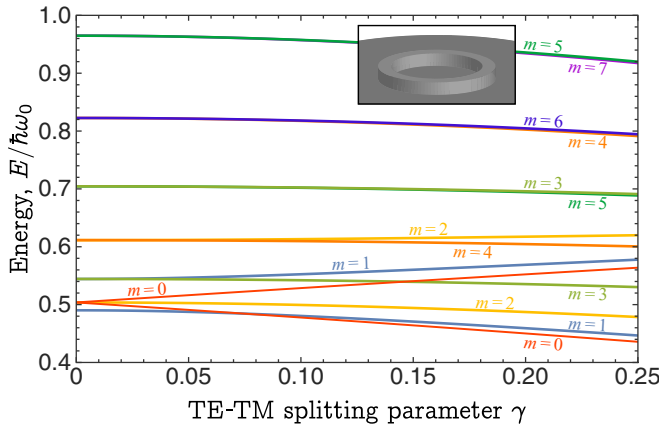
FIG. 2. Energy levels for polaritons moving in the ring (see the beginning of Sec. IV for details). The schematic geometry of the microcavity is shown in the inset. The confining frequency in the radial direction $\omega_0 = 40\hbar/m^*a^2$, where a is the radius of the ring.

is the ground state for $\gamma = 0$. As a result, the ground state changes at some critical value of SOC parameter γ_c and the lowest-energy azimuthal vortex becomes the ground state for $\gamma > \gamma_c$. In the case of parabolic potential this happens at a very high value of $\gamma_c \simeq 0.918$ [not shown in Fig. 1(c)].

The effect of ground-state change is more pronounced in the case of polariton confinement in a hard-wall disk. For the case of Rashba SOC this problem has been solved in Refs. [39–41]. The hard-wall billiards, in general, and an axially symmetric disk trap, in particular, can be formed by excitation of polaritons along the perimeter by a spatially structured pump [42–44], so that the polaritons move freely inside the trap and are reflected from the boundary due to repulsion from the incoherent excitonic reservoir. The energy levels of polaritons in the disk are shown in Fig. 1(d). In this case the crossing of levels takes place at $\gamma_c \simeq 0.625$. This value is still too high as compared with typical values of $\gamma \sim 0.1$ in semiconductor microcavities [45]. Note, however, that the values of γ can be substantially bigger in microcavities with organic layers [46]. The effect of the ground-state change can be observed for small values of TE-TM splitting in the case of trapping polaritons in the ring, which is considered in the next section.

IV. POLARITONS IN THE RING

The energy levels for polaritons moving in the ring are presented in Fig. 2. The calculations have been carried out for

a simple model potential $U(r) = U_0[1 - 2(r/a)^2 + (r/a)^4]$, where a is the radius of the ring and U_0 defines the barrier in the center. Since quasi-1D motion is achieved in the limit of large $U_0 \gg \hbar^2/m^*a^2$, the levels shown in Fig. 2 are practically identical to the levels in harmonic approximation for the potential with

$$U(r) = \frac{1}{2}m^*\omega_0^2(r-a)^2, \tag{10}$$

where $\omega_0 = \sqrt{8U_0/m^*}$. This frequency is used to scale the energy levels in Fig. 2. One can observe that the crossing of low-energy levels takes place at a rather small value of the TE-TM splitting parameter, $\gamma_c \simeq 0.074$ for $\omega_0 m^*a^2/\hbar = 40$. Moreover, the crossing value γ_c decreases further with increase in the ring confinement frequency. The effect of TE-TM splitting on the high-energy levels is much less pronounced. There is approximate additional degeneracy of the levels with large winding numbers m. Due to the form of the wave function defined by Eqs. (2) and (5), where the angular momenta of the $\psi_{\pm 1}$ components differ by 2, the separations of the first (lowest energy) level with $m = 6$ and the second level with $m = 4$, as well as of the second $m = 5$ level and the first $m = 7$ level, are nearly invisible.

To get a better understanding of the effect of SOC on the low-energy levels, it is convenient to derive the effective Hamiltonian for the quasi-1D angular motion of a polariton in the ring. This Hamiltonian can be particularly useful for the analysis of polariton condensation in the ring geometry, spontaneous azimuthal currents [47], formations of space-time periodic polarization patterns [24,35,48], and annular Josephson vortices [49,50]. The annular Hamiltonian can be obtained in adiabatic approximation by averaging over the appropriate radial wave function. In the presence of TE-TM splitting of polariton bands this procedure should be done carefully, since there are two masses, m_t and m_l, and it is not evident which one should be used for calculation of the radial component of the wave function. (Obtaining the annular Hamiltonian for the case of Rashba SOC is also error prone; see the discussion in Ref. [51].)

The derivation can be conveniently carried out using the equations for the radial ψ_r and azimuthal ψ_ϕ components of the vector function $\boldsymbol{\psi}$,

$$\psi_r = \frac{1}{\sqrt{2}}(e^{i\phi}\psi_{+1} + e^{-i\phi}\psi_{-1}), \tag{11a}$$

$$\psi_\phi = \frac{i}{\sqrt{2}}(e^{i\phi}\psi_{+1} - e^{-i\phi}\psi_{-1}). \tag{11b}$$

From Eq. (1) one obtains

$$-\frac{\hbar^2}{2}\left[\frac{1}{m_l}\frac{\partial}{\partial r}\left(\frac{\partial}{\partial r} + \frac{1}{r}\right) + \frac{1}{m_t r^2}\frac{\partial^2}{\partial \phi^2}\right]\psi_r + \frac{\hbar^2}{m^*}\left[\frac{1}{r^2}\frac{\partial}{\partial \phi} - \frac{\gamma}{r}\frac{\partial^2}{\partial r \partial \phi}\right]\psi_\phi = [E - U(r,\phi)]\psi_r, \tag{12a}$$

$$-\frac{\hbar^2}{m^*}\left[\frac{1}{r^2}\frac{\partial}{\partial \phi} + \frac{\gamma}{r}\frac{\partial^2}{\partial r \partial \phi}\right]\psi_r - \frac{\hbar^2}{2}\left[\frac{1}{m_t}\frac{\partial}{\partial r}\left(\frac{\partial}{\partial r} + \frac{1}{r}\right) + \frac{1}{m_l r^2}\frac{\partial^2}{\partial \phi^2}\right]\psi_\phi = [E - U(r,\phi)]\psi_\phi. \tag{12b}$$

Application of adiabatic approximation implies separation of fast motion in the radial direction and slow annular motion, $\psi_r = R_r(r)\Phi_r(\phi)$ and $\psi_\phi = R_\phi(r)\Phi_\phi(\phi)$, and it is clear from

Eqs. (12a) and (12b) that the radial part R_r is defined by Eq. (9) with the longitudinal mass m_l, while the azimuthal part R_ϕ is given by the same equation, but with the transverse

mass m_t. For parabolic trapping potential (10), averaging over radial components can be carried out using the scaling relation between R_r and R_ϕ. The resulting equations for the angular components are

$$\left[E_l(\gamma) + \frac{\hbar^2 k_\phi^2}{2m_t}\right]\Phi_r + i\varkappa(\gamma)\frac{\hbar^2 k_\phi}{m^* a}\Phi_\phi = E\Phi_r, \qquad (13a)$$

$$-i\varkappa(\gamma)\frac{\hbar^2 k_\phi}{m^* a}\Phi_r + \left[E_t(\gamma) + \frac{\hbar^2 k_\phi^2}{2m_l}\right]\Phi_\phi = E\Phi_\phi. \qquad (13b)$$

Here, $k_\phi = -i\partial/a\partial\phi$ is the annular wave vector; $E_t(\gamma) = \varepsilon_0\sqrt{1-\gamma}$ and $E_l(\gamma) = \varepsilon_0\sqrt{1+\gamma}$ with $\varepsilon_0 \simeq (\hbar\omega_0/2) + (\hbar^2/2m^* a^2)$ are the energies of the vortex solutions shown in Figs. 1(a) and 1(b), respectively, and they are plotted in Fig. 2 as $m = 0$ solutions. Finally, the coefficient

$$\varkappa(\gamma) = \sqrt{\frac{2(1-\gamma^2)^{1/4}}{(1+\gamma)^{1/2} + (1-\gamma)^{1/2}}} \qquad (14)$$

appears due to the overlap of the radial functions $R_r(r)$ and $R_\phi(r)$. If the difference in the longitudinal and transverse masses is not too extreme, this coefficient is very close to 1, and it can be safely omitted from Eqs. (13a) and (13b).

The energy levels E_m can be found by replacing $k_\phi \to m/a$ and Eqs. (13a) and (13b) describe very well these levels in the adiabatic limit $\hbar^2 m^2/2m^* a^2 \ll \varepsilon_0$. For small $|\gamma| \ll 1$ one has

$$E_m = \varepsilon_0 + \frac{\hbar^2 m^2}{2m^* a^2} \pm \sqrt{\left(\frac{\gamma\varepsilon_0}{2}\right)^2 + \left(\frac{\hbar^2 m}{m^* a^2}\right)^2}. \qquad (15)$$

It is evident that even weak TE-TM splitting cannot be neglected when considering the motion of polaritons in the ring, since the small parameter γ is multiplied by a large energy ε_0 that scales the quantization of levels in the radial direction. The point of the level crossing corresponds to a very small $\gamma_c \ll 1$, and it can be obtained from (15) that

$$\gamma_c = \frac{3\hbar}{m^* a^2 \omega_0}. \qquad (16)$$

Another way to view these results relies on the properties of polariton dispersion in a quantum wire. The 2×2 Hamiltonian defined by Eqs. (13a) and (13b) implies that in the straight wire, i.e., for $a \to \infty$, there are two independent modes. A polariton can possess transverse polarization, in which case it is quantized in the wire with longitudinal mass and moves along the wire with the transverse mass, or vice versa. For a curved wire, however, these two modes are coupled. The coupling is linear in the wave vector, similarly to the Rashba coupling. Remarkably, the coupling strength for polaritons is proportional to the curvature of the wire a^{-1} and can therefore be controlled [52].

The polariton bands in the wire are shown in Fig. 3. One can see that there is qualitative change in the lowest band dispersion with increasing radius of the wire, related to the disappearance of two side minima. This corresponds to the change from the double degenerate ground state to the nondegenerate one. Note also that, in contrast to the electron case, the spin-orbital coupling produces splitting of the bands at $k = 0$.
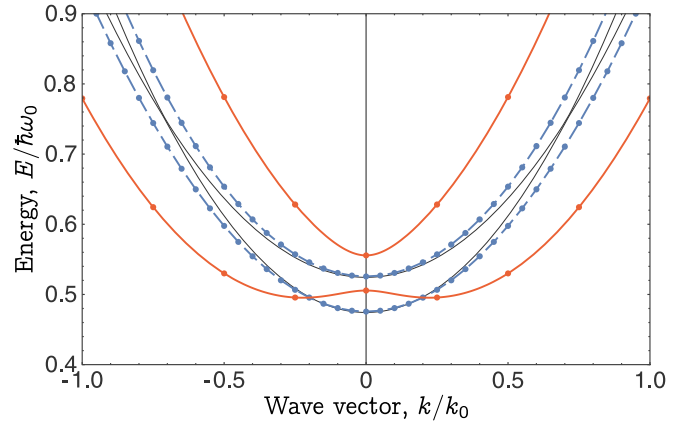

FIG. 3. The dispersion of polariton bands in the wire for the TE-TM splitting parameter $\gamma = 0.1$ and different values of the wire radius a. Quantized values of the wave vector, which is given in units of $k_0 = \sqrt{m^*\omega_0/\hbar}$, are shown by dots. Thick solid and dashed lines correspond to $k_0 a = 4$ and $k_0 a = 20$, respectively. Thin solid lines show the dispersion in the straight wire ($a \to \infty$).

The polarization vortex is expected to be the ground state for the polariton rings investigated in Ref. [53], with a ring radius of $a = 50\ \mu$m and the localization length in the radial direction corresponding to $\sqrt{\hbar/m\omega_0} \simeq 4\ \mu$m. In this case, the level crossing value $\gamma_c \simeq 0.019$. For the TE-TM splitting parameter $\gamma = 0.1$, the distance to the first excited ($m = 1$) level is about $0.2\ \mu$eV, which is about an order of magnitude smaller than the dissipation broadening of the levels at the polariton lifetime $\tau \sim 200$ ps [35]. To improve the level resolution, it is necessary to increase localization in the radial direction. Efficient spin-flip relaxation is also necessary for spontaneous formation of the polarization vortices shown in Figs. 1(a) and 1(b). However, the polarization vortices can be directly excited with corresponding Laguerre-Gaussian beams. Depending on the sign of γ, one of them will be stable, both topologically and energetically, while the other should decay into the lower-energy polariton states. In general, at least three polariton states, the $m = 0$ singlet and the $m = 1$ doublet, should be taken into account considering polariton condensation in the presence of dissipation and spin-dependent polariton-polariton interaction.

V. CONCLUSIONS

Spin-orbital coupling (TE-TM splitting) for exciton-polaritons has a pronounced effect on their levels in traps and can change the symmetry of the ground state. The effect is especially strong for polaritons localized in the ring traps, where the effective 1D Hamiltonian of their motion possesses linear-in-the-wave-vector coupling between two polarization modes, similarly to the case of Rashba SOC. In this case, even weak SOC cannot be neglected.

The crossover from the double-degenerate ground state in the ring to the singlet polarization-vortex state occurs at rather small values of the SOC coupling strength, which is inversely proportional to the confining frequency of the 1D wire and to the square of the ring radius; see Eq. (16). As a result, the polaritons form the polarization-vortex singlet state in

large-radius rings, while the ground state in small-sized rings is a doublet without a particular polarization structure.

The importance of TE-TM splitting for the polariton motion in curved wires discussed in this paper is only one little example from the rich world of different physical phenomena based upon the existence of linear-in-the-wave-vector spin-orbital coupling in solids. The seed that gave rise to this magnificent tree of new ideas and effects was planted by Emmanuel Rashba more than 60 years ago. It is spectacular how, after all these years, this tree continues to grow and bear new fruit.

[1] E. I. Rashba and V. I. Sheka, Symmetry of energy bands in crystals of wurtzite type II. Symmetry of bands with spin-orbit interaction included, Fiz. Tverd. Tela **2**, 162 (1959) available as Supplemental Material to the paper by G. Bihlmayer, O. Rader, and R. Winkler, Focus on the Rashba effect, New J. Phys. **17**, 050202 (2015).

[2] E. I. Rashba, Properties of semiconductors with an extremum loop. 1. Cyclotron and combinational resonance in a magnetic field perpendicular to the plane of the loop, Fiz. Tverd. Tela **2**, 1224 (1960) [Sov. Phys. Solid State **2**, 1109 (1960)].

[3] E. I. Rashba and V. I. Sheka, Combinational resonance of zonal electrons in crystals having a zinc blende lattice, Fiz. Tverd. Tela **3**, 1735 (1961) [Sov. Phys. Solid State **3**, 1257 (1961)].

[4] E. I. Rashba and V. I. Sheka, Electric-dipole spin resonances, in *Landau Level Spectroscopy*, Modern Problems in Condensed Matter Sciences Vol. 27.1, edited by G. Landwehr and E. I. Rashba (North Holland, Amsterdam, 1990), Chap. 4, pp. 131–206.

[5] F. T. Vas'ko, Spin splitting in the spectrum of two-dimensional electrons due to the surface potential, Pis'ma Zh. Eksp. Teor. Fiz. **30**, 574 (1979) [JETP Lett. **30**, 541 (1979)].

[6] Yu. A. Bychkov and E. I. Rashba, Properties of a 2D electron gas with lifted spectral degeneracy, Pis'ma Zh. Eksp. Teor. Fiz. **39**, 66 (1984) [JETP Lett. **39**, 78 (1984)].

[7] G. Dresselhaus, Spin-orbit coupling eeffects in zinc bblende structures, Phys. Rev. **100**, 580 (1955).

[8] E. I. Rashba and Al. L. Efros, Orbital Mechanisms of Electron-Spin Manipulation by an Electric Field, Phys. Rev. Lett. **91**, 126405 (2003).

[9] I. Žutić, J. Fabian, and S. Das Sarma, Spintronics: Fundamentals and applications, Rev. Mod. Phys. **76**, 323 (2004).

[10] D. D. Awschalom, D. Loss, and N. Samarth, *Semiconductor Spintronics and Quantum Computation* (Springer, Berlin, 2013).

[11] A. Manchon, H. C. Koo, J. Nitta, S. M. Frolov, and R. A. Duine, New perspectives for Rashba spin-orbit coupling, Nat. Mater. **14**, 871 (2015).

[12] S. I. Pekar, The theory of electromagnetic waves in a crystal in which excitons are produced, Zh. Eksp. Teor. Fiz. **33**, 1022 (1957) [Sov. Phys. JETP **6**, 785 (1958)].

[13] It is difficult to indicate who has put forward this argument for exciton polaritons first. I personally learned it from S. I. Pekar in 1984.

[14] K. Huang, *Statistical Mechanics*, 2nd ed. (Wiley, New York, 1987).

[15] J. Klaers, J. Schmitt, F. Vewinger, and M. Weitz, Bose-Einstein condensation of photons in an optical microcavity, Nature (London) **468**, 545 (2010).

[16] A. V. Kavokin, J. J. Baumberg, G. Malpuech, and F. P. Laussy, *Microcavities*, 2nd ed. (Oxford University Press, Oxford, 2017).

[17] J. Kasprzak, M. Richard, S. Kundermann, A. Baas, P. Jeambrun, J. M. J. Keeling, F. M. Marchetti, M. H. Szymańska, R. André, J. L. Staehli, V. Savona, P. B. Littlewood, B. Deveaud, and L. S. Dang, Bose-Einstein condensation of exciton polaritons, Nature (London) **443**, 409 (2006).

[18] R. Balili, V. Hartwell, D. Snoke, L. Pfeiffer, and K. West, Bose-Einstein condensation of microcavity polaritons in a trap, Science **316**, 1007 (2007).

[19] J. J. Baumberg, A. V. Kavokin, S. Christopoulos, A. J. D. Grundy, R. Butté, G. Christmann, D. D. Solnyshkov, G. Malpuech, G. Baldassarri Höger von Högersthal, E. Feltin, J.-F. Carlin, and N. Grandjean, Spontaneous Polarization Buildup in a Room-Temperature Polariton Laser, Phys. Rev. Lett. **101**, 136409 (2008).

[20] A. Kavokin, G. Malpuech, and M. Glazov, Optical Spin Hall Effect, Phys. Rev. Lett. **95**, 136601 (2005).

[21] C. Leyder, M. Romanelli, J. P. Karr, E. Giacobino, T. C. H. Liew, M. M. Glazov, A. V. Kavokin, G. Malpuech, and A. Bramati, Observation of the optical spin Hall effect, Nat. Phys. **3**, 628 (2007).

[22] I. A. Shelykh, G. Pavlovic, D. D. Solnyshkov, and G. Malpuech, Proposal for a Mesoscopic Optical Berry-Phase Interferometer, Phys. Rev. Lett. **102**, 046407 (2009).

[23] E. S. Sedov, Y. G. Rubo, and A. V. Kavokin, *Zitterbewegung* of exciton-polaritons, Phys. Rev. B **97**, 245312 (2018).

[24] E. Sedov, I. Sedova, S. Arakelian, and A. Kavokin, Polygonal patterns of confined light, Opt. Lett. **46**, 1836 (2021).

[25] I. A. Shelykh, A. V. Kavokin, Y. G. Rubo, T. C. H. Liew, and G. Malpuech, Polariton polarization-sensitive phenomena in planar semiconductor microcavities, Semicond. Sci. Technol. **25**, 013001 (2010).

[26] C. E. Whittaker, T. Dowling, A. V. Nalitov, A. V. Yulin, B. Royall, E. Clarke, M. S. Skolnick, I. A. Shelykh, and D. N. Krizhanovskii, Optical analogue of Dresselhaus spin-orbit interaction in photonic graphene, Nat. Photonics **15**, 193 (2021).

[27] R. G. Sachs, *The Physics of Time Reversal* (University of Chicago Press, Chicago, 1987).

[28] K. Rechcińska, M. Król, R. Mazur, P. Morawiak, R. Mirek, K. Łempicka, W. Bardyszewski, M. Matuszewski, P. Kula, W. Piecek, P. G. Lagoudakis, B. Piętka, and J. Szczytko, Engineering spin-orbit synthetic Hamiltonians in liquid-crystal optical cavities, Science **366**, 727 (2019).

[29] B. A. Bernevig, J. Orenstein, and S.-C. Zhang, Exact SU(2) Symmetry and Persistent Spin Helix in a Spin-Orbit Coupled System, Phys. Rev. Lett. **97**, 236601 (2006).

[30] M. Król, K. Rechcińska, H. Sigurdsson, P. Oliwa, R. Mazur, P. Morawiak, W. Piecek, P. Kula, P. G. Lagoudakis, M. Matuszewski, W. Bardyszewski, B. Piętka, and J. Szczytko, Realizing Optical Persistent Spin Helix and Stern-Gerlach Deflection in an Anisotropic Liquid Crystal Microcavity, Phys. Rev. Lett. **127**, 190401 (2021).

[31] F. Manni, K. G. Lagoudakis, T. C. H. Liew, R. André, and B. Deveaud-Plédran, Spontaneous Pattern Formation in a Polariton Condensate, Phys. Rev. Lett. **107**, 106401 (2011).

[32] A. Dreismann, P. Cristofolini, R. Balili, G. Christmann, F. Pinsker, N. G. Berloff, Z. Hatzopoulos, P. G. Savvidis, and J. J. Baumberg, Coupled counterrotating polariton condensates in optically defined annular potentials, Proc. Natl. Acad. Sci. U. S. A. **111**, 8770 (2014).

[33] G. Liu, D. W. Snoke, A. Daley, L. N. Pfeiffer, and K. West, A new type of half-quantum circulation in a macroscopic polariton spinor ring condensate, Proc. Natl. Acad. Sci. U. S. A. **112**, 2676 (2015).

[34] V. A. Lukoshkin, V. K. Kalevich, M. M. Afanasiev, K. V. Kavokin, Z. Hatzopoulos, P. G. Savvidis, E. S. Sedov, and A. V. Kavokin, Persistent circular currents of exciton-polaritons in cylindrical pillar microcavities, Phys. Rev. B **97**, 195149 (2018).

[35] S. Mukherjee, V. K. Kozin, A. V. Nalitov, I. A. Shelykh, Z. Sun, D. M. Myers, B. Ozden, J. Beaumariage, M. Steger, L. N. Pfeiffer, K. West, and D. W. Snoke, Dynamics of spin polarization in tilted polariton rings, Phys. Rev. B **103**, 165306 (2021).

[36] E. Estrecho, M. Pieczarka, M. Wurdack, M. Steger, K. West, L. N. Pfeiffer, D. W. Snoke, A. G. Truscott, and E. A. Ostrovskaya, Low-Energy Collective Oscillations and Bogoliubov Sound in an Exciton-Polariton Condensate, Phys. Rev. Lett. **126**, 075301 (2021).

[37] K. Y. Bliokh, F. J. Rodríguez-Fortuño, F. Nori, and A. V. Zayats, Spin-orbit interactions of light, Nat. Photonics **9**, 796 (2015).

[38] E. S. Sedov, Y. G. Rubo, and A. V. Kavokin, Polariton polarization rectifier, Light: Sci. Appl. **8**, 79 (2019).

[39] E. I. Rashba, Quantum nanostructures in strongly spin-orbit coupled two-dimensional systems, Phys. Rev. B **86**, 125319 (2012).

[40] E. N. Bulgakov and A. F. Sadreev, Spin polarization in quantum dots by radiation field with circular polarization, JETP Lett. **73**, 505 (2001).

[41] E. Tsitsishvili, G. S. Lozano, and A. O. Gogolin, Rashba coupling in quantum dots: An exact solution, Phys. Rev. B **70**, 115316 (2004).

[42] A. Askitopoulos, H. Ohadi, A. V. Kavokin, Z. Hatzopoulos, P. G. Savvidis, and P. G. Lagoudakis, Polariton condensation in an optically induced two-dimensional potential, Phys. Rev. B **88**, 041308(R) (2013).

[43] P. Cristofolini, A. Dreismann, G. Christmann, G. Franchetti, N. G. Berloff, P. Tsotsis, Z. Hatzopoulos, P. G. Savvidis, and J. J. Baumberg, Optical Superfluid Phase Transitions and Trapping of Polariton Condensates, Phys. Rev. Lett. **110**, 186403 (2013).

[44] T. Gao, E. Estrecho, K. Y. Bliokh, T. C. H. Liew, M. D. Fraser, S. Brodbeck, M. Kamp, C. Schneider, S. Höfling, Y. Yamamoto, F. Nori, Y. S. Kivshar, A. G. Truscott, R. G. Dall, and E. A. Ostrovskaya, Observation of non-Hermitian degeneracies in a chaotic exciton-polariton billiard, Nature (London) **526**, 554 (2015).

[45] K. V. Kavokin, I. A. Shelykh, A. V. Kavokin, G. Malpuech, and P. Bigenwald, Quantum Theory of Spin Dynamics of Exciton-Polaritons in Microcavities, Phys. Rev. Lett. **92**, 017401 (2004).

[46] S. Stelitano, S. Savasta, S. Patané, G. De Luca, and L. Monsù Scolaro, Origin of giant polarization splitting in high quality organic microcavities, J. Appl. Phys. **106**, 033102 (2009).

[47] A. V. Nalitov, T. C. H. Liew, A. V. Kavokin, B. L. Altshuler, and Y. G. Rubo, Spontaneous Polariton Currents in Periodic Lateral Chains, Phys. Rev. Lett. **119**, 067406 (2017).

[48] A. V. Nalitov, H. Sigurdsson, S. Morina, Y. S. Krivosenko, I. V. Iorsh, Y. G. Rubo, A. V. Kavokin, and I. A. Shelykh, Optically trapped polariton condensates as semiclassical time crystals, Phys. Rev. A **99**, 033830 (2019).

[49] A. Muñoz Mateo, Y. G. Rubo, and L. A. Toikka, Long Josephson junctions with exciton-polariton condensates, Phys. Rev. B **101**, 184509 (2020).

[50] I. Chestnov, A. Yulin, I. A. Shelykh, and A. Kavokin, Dissipative Josephson vortices in annular polariton fluids, Phys. Rev. B **104**, 165305 (2021).

[51] F. E. Meijer, A. F. Morpurgo, and T. M. Klapwijk, One-dimensional ring in the presence of Rashba spin-orbit interaction: Derivation of the correct Hamiltonian, Phys. Rev. B **66**, 033107 (2002).

[52] Note that weak coupling between these modes, also linear in the wave vector, can appear in a straight but asymmetric wire, see I. A. Shelykh, A. V. Nalitov, and I. V. Iorsh, Optical analog of Rashba spin-orbit interaction in asymmetric polariton waveguides, Phys. Rev. B **98**, 155428 (2018).

[53] S. Mukherjee, D. M. Myers, R. G. Lena, B. Ozden, J. Beaumariage, Z. Sun, M. Steger, L. N. Pfeiffer, K. West, A. J. Daley, and D. W. Snoke, Observation of nonequilibrium motion and equilibration in polariton rings, Phys. Rev. B **100**, 245304 (2019).